Available online at www.sciencedirect.com
ScienceDirect
International Journal of Heat and Mass Transfer 50 (2007) 2895–2904
International Journal of HEAT and MASS TRANSFER
www.elsevier.com/locate/ijhmt

# 3-Dimensional numerical optimization of silicon-based high performance parallel microchannel heat sink with liquid flow

J. Li [a], G.P. Peterson [b,*]

[a] Department of Mechanical, Aerospace and Nuclear Engineering, Rensselaer Polytechnic Institute, 110 8th Street, Troy, NY 12180, United States
[b] Department of Mechanical Engineering, University of Colorado, Boulder, CO 80309, United States

Received 16 July 2006; received in revised form 6 January 2007
Available online 27 March 2007

**Abstract**

A full 3-dimensional (3D) conjugate heat transfer model has been developed to simulate the heat transfer performance of silicon-based, parallel microchannel heat sinks. A semi-normalized 3-dimensional heat transfer model has been developed, validated and used to optimize the geometric structure of these types of microheat sinks. Under a constant pumping power of 0.05 W for a water-cooled microheat sink, the optimized geometric parameters of the structure as determined by the model were a pitch of 100 μm, a channel width of 60 μm and a channel depth of about 700 μm. The thermal resistance of this optimized microheat sink was calculated for different pumping powers based on the full 3D conjugate heat transfer model and compared with the initial experimental results obtained by Tuckerman and Pease in 1981. This comparison indicated that for a given pumping poser, the overall cooling capacity could be enhanced by more than 20% using the optimized spacing and channel dimensions. The overall thermal resistance was 0.068 °C/W for a pumping power of 2 W.


*Keywords:* Microchannel; Numerical simulation; Heat transfer; Optimization; Microelectronic cooling

## 1. Introduction

Recent advances in microelectromechanical devices (MEMS), advances in very large-scale integration (VLSI) technologies and the associated microminiaturization of semiconductor devices in general, has led to significant increases in the packaging densities and associated heat fluxes generated within these devices. These increases are typified by the projections in the International Technology Roadmap for Semiconductors (ITRS) [1] that indicates that volumetric heat generation rates will approach $3.3 \times 10^4$ W/mm$^3$. This level of power generation will require that junction-to-ambient thermal resistances be below 0.14 °C/W in order to meet the suggested maximum junction temperatures of 85 °C required for long-term, high-performance operation of these devices. One of the possible methods for removing the resulting high heat fluxes, is to utilize microchannel heat sinks with or without phase change, fabricated as an integral part of the silicon wafers. This approach was first presented over 25 years ago by Tuckerman and Pease [2]. Since that time, numerous investigations have been conducted using a variety of designs and geometric configurations. However, review of the existing experimental results indicates that in the vast majority of these investigations, the geometries evaluated were selected arbitrarily or based upon ease of fabrication, rather than through the use of some sort of theoretical or computational analysis to determine the optimal configuration. As a result, the thermal performance of these non-optimal devices was well below what could be achieved with relatively small changes in the geometry and that the current technology was sufficiently robust to allow the fabrication of these optimized geometries.

While many of the initial investigations were performed on non-optimal geometries, the results clearly indicated a

* Corresponding author. Tel.: +1 303 4928908; fax: +1 303 4928866.
*E-mail address:* Bud.Peterson@colorado.edu (G.P. Peterson).

0017-9310/$ - see front matter © 2007 Elsevier Ltd. All rights reserved.
doi:10.1016/j.ijheatmasstransfer.2007.01.019

**Nomenclature**

| | |
|---|---|
| $a$ | thermal diffusivity |
| $A$ | total surface area of microchannel |
| $A_c$ | area of cross-section of microchannel |
| $C_P$ | specific heat |
| $D_h$ | hydraulic diameter |
| $f$ | friction factor |
| $H$ | height of channel |
| $h$ | convective heat transfer coefficient |
| $\dot{m}$ | mass flow rate |
| $N$ | number of channels |
| $P$ | pressure |
| $\overline{P}$ | pumping power |
| $q_w$ | heat flux |
| $Re$ | Reynolds number |
| $T$ | temperature |
| $u$ | $x$-direction velocity of liquid |
| $U$ | dimensionless velocity |
| $\dot{V}$ | total volume flow rate |
| $V$ | vector of velocity |
| $W$ | width of channel |
| $W_{pitch}$ | width of pitch |

*Greek symbols*

| | |
|---|---|
| $\theta$ | dimensionless temperature |
| $\delta$ | thickness of the substrate bottom wall |
| $\lambda$ | conductivity |
| $\rho$ | density |
| $\mu$ | dynamic viscosity |
| $\upsilon$ | kinetic viscosity |
| $\Gamma$ | periphery of the inner wall of channel |

*Subscripts*

| | |
|---|---|
| b | bulk liquid |
| l | liquid |
| $m$ | mean value |
| w | substrate |

relationship between the cross-sectional aspect ratio and the flow friction and convective heat transfer for both laminar and turbulent conditions. In a majority of cases, silicon-based MEMS technology was used to create microchannels within silicon wafers that had trapezoidal or triangular cross-sections (anisotropic wet etching on $\langle 100 \rangle$ wafer) or rectangular cross-sections (DRIE or wet etching on $\langle 110 \rangle$ wafers) as opposed to more traditional circular cross-sections. In addition, in most cases, heat was added to the bottom of the wafer, resulting in non-symmetrical heat addition to the channel periphery.

Recently, efforts have been underway to analyze the possible optimal structure for these parallel microchannel heat sinks [3–10]. Among these optimization works, two principle methods were adopted: one is the fin efficiency method [3–6] and the second is a numerical computation method [7–10]. It is interesting to note that optimal geometries suggested by these two approaches were seldom similar. This may be due to the fact that the fin efficiency method requires a number of assumptions, which may vary from one investigator to the next and hence, reduce the accuracy of the results, for example (i) the assumption of the heat transfer coefficient which could vary for different investigations, (ii) the assumption of a constant temperature difference between the solid and the bulk fluid, and (iii) the assumption that the axial heat conduction is negligible. Alternatively, in the majority of the numerical approaches developed, a very simple 2-dimensional heat transfer model was used to determine the optimal value [7,8] or in some cases, a very coarse mesh was adopted [9] for use in the numerical approach. Recently, Li and Peterson [10] proposed a rigorous, 3-dimensional semi-normalized numerical method to explore the optimal geometry of the parallel microchannel heat sinks and demonstrated that on a silicon wafer with a typical thickness of 450 μm, the configurations first used by Tuckerman and Pease [2] and by Kawano et al. [11], were quite close to the optimized values predicted by the numerical model. Nevertheless, the ultimate optimal geometry was not achieved due to the constraint of the wafer thickness of 450 μm.

In the current investigation, a detailed full 3-dimensional numerical simulation of the conjugate heat transfer problem was conducted in order to analyze the effect of the geometry of these silicon-based microchannel heat sinks on the overall heat transfer performance and to determine the optimal structure of the microheat sink under the assumption of a constant pumping power. The microheat sinks evaluated in this investigation, consist of a 10 mm long and 10 mm wide silicon substrate (1 $cm^2$). Using this configuration, the effects of the microchannel geometry on the temperature distribution in the heat sink (or the thermal resistance) are investigated. With the optimized geometry, the heat transfer performance of the microchannel heat sink as determined by the variation in the thermal resistance was then calculated for different pumping powers and compared with the existing experimental results. In addition, a number of microfabrication issues are also presented and discussed in terms of the feasibility of fabrication of the resulting optimized, deep trench microchannel heat sinks.

## 2. 3-D conjugate heat transfer modeling in microheat sinks

Rectangular microchannels can be fabricated using silicon wafers with aspect ratios, $H/W$, of up to 20:1 using DRIE and 6:1 using KOH wet etching techniques, subject to a number of constraints. These constraints are the result of issues related to the stress and deflection under high

pressure and the microfabrication process itself. Typically, a minimum thickness of 100 μm for the external channel walls is the widely accepted value, based upon both experimental [2,11] and analytical [9,10] optimization techniques. In addition, the maximum practical aspect ratio should be less than 20:1 due to the degree of difficulty and the economy in microfabrication.

A schematic of the geometry of parallel microchannel heat sinks investigated and evaluated in the current investigation is shown in Fig. 1. In this configuration, a uniform power density was applied to the bottom of the heat sink with the objective being to determine the optimal design. This optimal design was determined by minimizing the thermal resistance between the hottest point on the heat sink and the coldest point in the coolant and is referred to as the global thermal resistance or the "junction" thermal resistance, when subjected to a specified heat input and pumping power.

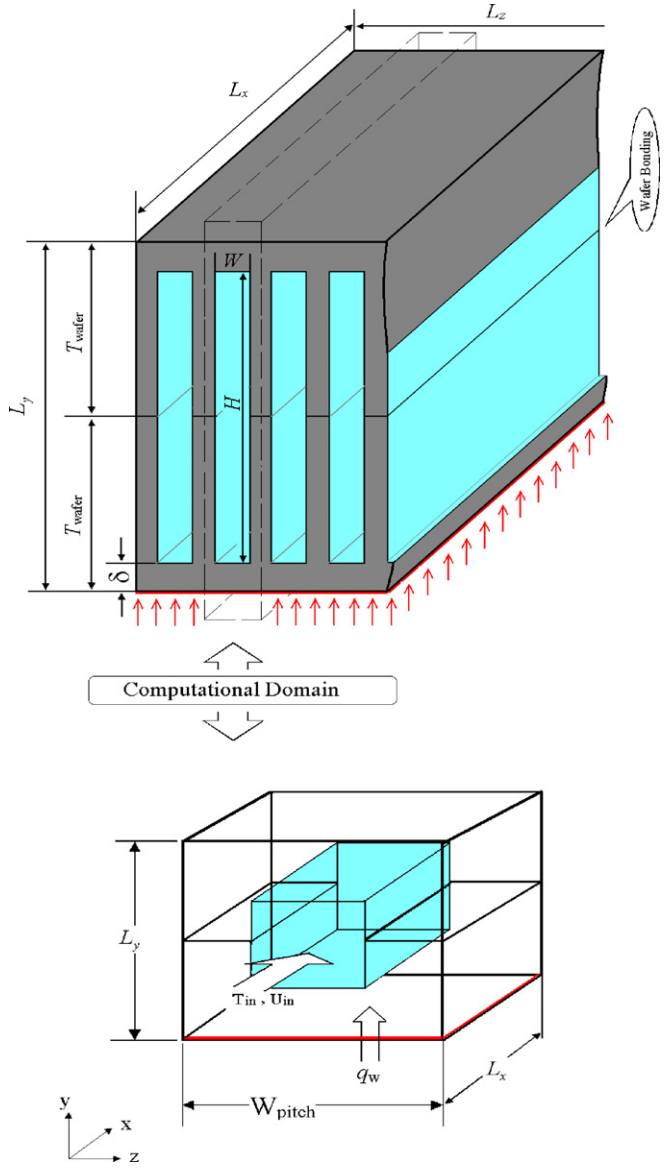


Fig. 1. Structure of a parallel microchannel heat sink and the 3D numerical domain.

To establish this value, the pumping power, $\overline{P}$, is assumed to be held at a constant value. Under such a constraint, an optimal analysis could be carried out by comparing the thermal resistance for different configurations, to determine how each of the dimensional parameters affects the overall thermal performance. This pumping power, $\overline{P}$, is defined as

$$\overline{P} = \dot{V} \cdot \Delta P = N \cdot u_m \cdot A_c \cdot \Delta P \tag{1}$$

where $\dot{V}$ is the total volume flow rate; $N$ is the number of channels; $u_m$ is the mean velocity in the channel; $A_c$ is the area of the cross-section of the channel; and $\Delta P$ is the pressure drop across the channel. This expression and approach has been widely used by previous researchers [8–10].

In the current investigation, referring to Fig. 1, the length $L_x$ and the width $L_z$ of the microheat sink were chosen to be 10 mm × 10 mm (1 cm$^2$). The thicknesses of the silicon wafers evaluated vary based upon the depth of the channel being investigated. The structure of the microchannel heat sink can be configured by bonding two wafers together with half-height channels fabricated on each wafer through direct silicon bonding methods with double side alignment [6] to achieve a deep trench channel with an aspect ratio well beyond 6:1. The use of this modified fabrication technique, will significantly reduce the difficulties associated with the microfabrication, since batch fabrication using low trench etching will save both time and cost, and will result in an improved channel shape if the undercutting is considered. In addition, these configurations can enhance the performance when compared to a glass cover with a low thermal conductivity, which has been the case for many previous investigations.

### 2.1. Full 3D conjugate heat transfer model

A full 3-dimensional (3D) conjugate heat transfer model of microchannel heat sinks has been developed. As shown in Fig. 1, this numerical model utilizes a cell with one rectangular channel as the computational domain, due to the symmetrical structure of the heat sink. If the gravitational force and the heat dissipation caused by viscosity are neglected for steady, incompressible, laminar flow, the governing equations for the liquid flow are

$$\frac{\partial u}{\partial x} + \frac{\partial v}{\partial y} + \frac{\partial w}{\partial z} = 0 \tag{2}$$

$$\rho\left(u\frac{\partial u}{\partial x} + v\frac{\partial u}{\partial y} + w\frac{\partial u}{\partial z}\right) = -\frac{\partial P}{\partial x} + \mu\left(\frac{\partial^2 u}{\partial x^2} + \frac{\partial^2 u}{\partial y^2} + \frac{\partial^2 u}{\partial z^2}\right) \tag{3a}$$

$$\rho\left(u\frac{\partial v}{\partial x} + v\frac{\partial v}{\partial y} + w\frac{\partial v}{\partial z}\right) = -\frac{\partial P}{\partial y} + \mu\left(\frac{\partial^2 v}{\partial x^2} + \frac{\partial^2 v}{\partial y^2} + \frac{\partial^2 v}{\partial z^2}\right) \tag{3b}$$

$$\rho\left(u\frac{\partial w}{\partial x} + v\frac{\partial w}{\partial y} + w\frac{\partial w}{\partial z}\right) = -\frac{\partial P}{\partial z} + \mu\left(\frac{\partial^2 w}{\partial x^2} + \frac{\partial^2 w}{\partial y^2} + \frac{\partial^2 w}{\partial z^2}\right) \tag{3c}$$

The hydrodynamic boundary conditions are

at the channel wall surface (no-slip), $u = v = w = 0$ (4a)

at the inlet, $x = 0$, $P_l = P_{in}$ (4b)

at the outlet, $x = L_x$, $P_l = P_{out}$ (4c)

The energy equation for the liquid is

$$\rho_l C_P \left( u\frac{\partial T_l}{\partial x} + v\frac{\partial T_l}{\partial y} + w\frac{\partial T_l}{\partial z} \right) = \lambda_l \left( \frac{\partial^2 T_l}{\partial x^2} + \frac{\partial^2 T_l}{\partial y^2} + \frac{\partial^2 T_l}{\partial z^2} \right) \tag{5}$$

and the heat conduction in the silicon wafer can be expressed as

$$\frac{\partial}{\partial x}\left(\lambda_w \frac{\partial T_w}{\partial x}\right) + \frac{\partial}{\partial y}\left(\lambda_w \frac{\partial T_w}{\partial y}\right) + \frac{\partial}{\partial z}\left(\lambda_w \frac{\partial T_w}{\partial z}\right) = 0 \tag{6}$$

which is subject to the following thermal boundary conditions

$$x = 0, \quad \text{if } (y,z) \in \text{channel } T_l = T_{in}, \text{ else} - \lambda_w \frac{\partial T_w}{\partial x} = 0 \tag{7a}$$

$$x = L_x, \quad \text{if } (y,z) \in \text{channel } -\lambda_l \frac{\partial T_l}{\partial x} = 0, \text{ else} - \lambda_w \frac{\partial T_w}{\partial x} = 0 \tag{7b}$$

$$y = 0, \quad -\lambda_w \frac{\partial T_w}{\partial y} = q_w \tag{7c}$$

$$y = L_y, \quad -\lambda_w \frac{\partial T_w}{\partial y} = 0 \tag{7d}$$

$$z = 0, \quad -\lambda_w \frac{\partial T_w}{\partial z} = 0 \tag{7e}$$

$$z = W_{pitch}, \quad -\lambda_w \frac{\partial T_w}{\partial z} = 0 \tag{7f}$$

$$\text{at the inner wall surface}, \quad -\lambda_w \left( \frac{\partial T_w(x)}{\partial n}\bigg|_\Gamma \right) = -\lambda_l \left( \frac{\partial T_l(x)}{\partial n}\bigg|_\Gamma \right) \tag{7g}$$

where Eq. (7c) gives the uniform heat flux boundary condition at the bottom wall of the wafer subjected to heating and Eqs. (7a), (7b), (7d)–(7f) assume no heat loss from the solid surfaces to the ambient surroundings at the boundaries. It should be noted that in actual applications, the heat loss from the solid substrate to the environment may be substantial and would need to be considered.

A mesh of $40(x) \times 45(y) \times 50(z)$ was adopted for the domain as shown in Fig. 1 with a non-uniform grid division. A SIMPLE method was applied to solve Eqs. (2) and (3) for steady, incompressible liquid flow with the boundary condition described in Eq. (4). Detailed information about the SIMPLE method can be found in Ref. [12]. And a line by line iteration method and a Tri-diagonal Matrix algorithm (TDMA) method were used, along with the Thomas algorithm and a successive under-relaxation iterative method, to solve the energy equations (5) and (6) with the boundary condition equation (7). The convergent criterion was set as

$$\sum\sum\sum \|\mathbf{V}(i,j,k)| - |\mathbf{V}_0(i,j,k)\| \leqslant 10^{-5} \quad \text{for the velocity} \tag{8}$$

$$\sum\sum\sum |T(i,j,k) - T_0(i,j,k)| \leqslant 5 \times 10^{-3} \quad \text{for the temperature} \tag{9}$$

The criterion for the temperature gives a mean square root error (MSRE) of $5 \times 10^{-8}$. A grid sensitivity analysis indicated that the accuracy of the velocity and temperature were dependent on the grid size and five different mesh sizes were evaluated $10(x) \times 25(y) \times 15(z)$, $20(x) \times 45(y) \times 25(z)$, $40(x) \times 45(y) \times 50(z)$, $20(x) \times 90(y) \times 100(z)$ and $40(x) \times 90(y) \times 100(z)$. It was found that the result of $40(x) \times 45(y) \times 50(z)$ will be different from $40(x) \times 90(y) \times 100(z)$ within 2% error for global thermal resistance if a MSRE of $5 \times 10^{-8}$ is set for the convergence. The results of $20(x) \times 45(y) \times 25(z)$ mesh (approximately 5% error) and $20(x) \times 90(y) \times 100(z)$ mesh (approximately 1% error) have been described previously in [10,13], respectively. Compared to the mesh selection, the convergence criterion is much more important for the accuracy of the computations.

Fig. 2 illustrates the dependence of the convergence value on the convergence criteria. The dashed line represents the possible temperature rise in the bulk fluid as determined through an energy conservation analysis. The difference between the results with a MSRE of $1 \times 10^{-8}$ and that obtained for a MSRE of $5 \times 10^{-8}$ is approximately 3%. To conserve computational time, an MSRE of $5 \times 10^{-8}$ was selected (even so, a single case will consume about 3–5 h on a Pentium IV 2.8G-CPU and 2G-Memory desktop computer). Using the relatively strict convergence conditions described in Eqs. (7) and (8), the results were found to be consistent with both mass and energy conservation, with a maximum total relative error of 6%. Furthermore, the truncation error involved in the

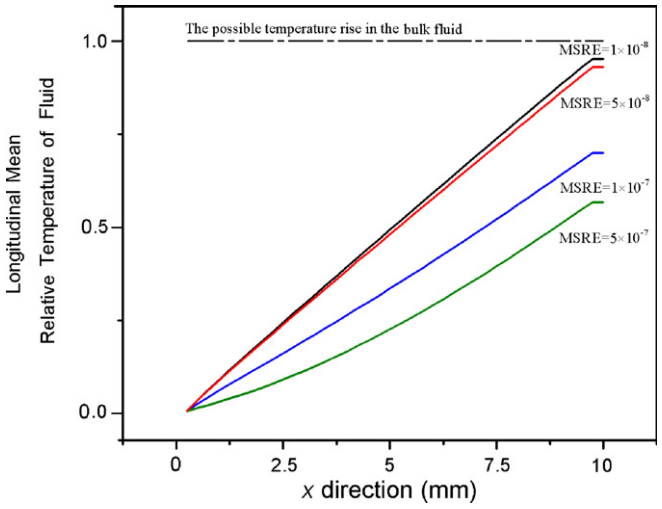


Fig. 2. The relation between the convergent values of longitudinal mean bulk temperature of fluid and the convergent criteria.

numerical calculations were almost the same magnitude for all of the calculations with similar grid dimensions.

Fig. 3a gives a typical result for the developing flow in microchannels under a pumping power of $\overline{P} = 0.05$ W in a channel with a height of 350 μm and a width of 60 μm. Fig. 3b shows the numerical results for a fully developed flow assumption under the same pumping power. The entrance length required for the formation of fully developed laminar flow is 4% of the total length, which roughly agrees with the prediction based upon the expression developed by Langhaar for a round tube [14].

$$\frac{L_e}{D_h} = 0.057 Re_D \tag{10}$$

Fig. 4 shows the comparison of the temperature distribution in the cross-section of a microheat sink at $z = W_{pitch}/2$ between the full 3D numerical simulation with Eqs. (2)–(7) and the simplified 3D numerical simulation with a fully developed assumption under a pumping power of $\overline{P} = 0.05$ W and a heat flux at the substrate bottom wall of $q_w = 100$ W/cm$^2$. The thickness of the silicon wafer is 450 μm and the thickness of the substrate bottom wall is $\delta = 100$ μm. The pitch is $W_{pitch} = 100$ μm, the width is $W = 60$ μm and the depth is $H = 350$ μm. From Fig. 4, it is apparent that the global thermal resistance is almost the same (with a difference less than 0.5%). It should be noted that at the entrance region, the heat transfer is a little higher for the full 3D numerical simulation than for the simplified 3D simulation due to the smaller boundary layer, as shown in Fig. 3a.

Based upon the preceding analysis, in the following optimization process the fully developed flow assumption will be adopted since: (i) under a small pumping power, the entrance length is quite small and can be neglected; (ii) under a small pumping power, this assumption will introduce a negligible error in the global thermal resistance; and (iii) most importantly, this assumption will allow a non-dimensional analysis approach feasible for the determination of the optimal geometry of the microchannel heat sink.

### 2.2. Semi-normalized simplified 3D conjugate heat transfer approach

Based upon the preceding analysis, a number of assumptions have been made in the following numerical optimization process:

(i) The flow is laminar and fully developed $u = u(y, z)$. Thus the momentum equation for the liquid flow is

$$\frac{\partial^2 u}{\partial y^2} + \frac{\partial^2 u}{\partial z^2} = -\frac{1}{\mu_l}\frac{\Delta P}{L_x} \tag{11}$$

and the energy equation for liquid becomes

$$u\frac{\partial T_l}{\partial x} = \frac{\lambda_l}{\rho_l C_P}\left(\frac{\partial^2 T_l}{\partial x^2} + \frac{\partial^2 T_l}{\partial y^2} + \frac{\partial^2 T_l}{\partial z^2}\right) \tag{12}$$

(ii) All material thermodynamic and hydrodynamic properties are constant. This assumption makes the non-dimensional analysis and optimal analysis in terms of thermal resistance possible, otherwise the results become case specific.

The detailed derivation of the semi-normalized 3D numerical approach has been given in [10]. However, for clarity, some of the more important processes are repeated here.

The cross-sectional mean velocity, $u_m$, can be used as the velocity scale, ($U(y,z) = u(y,z)/u_m$) and the Reynolds number can be defined as

$$Re_{D_h} = \frac{u_m D_h}{\upsilon} \tag{13}$$

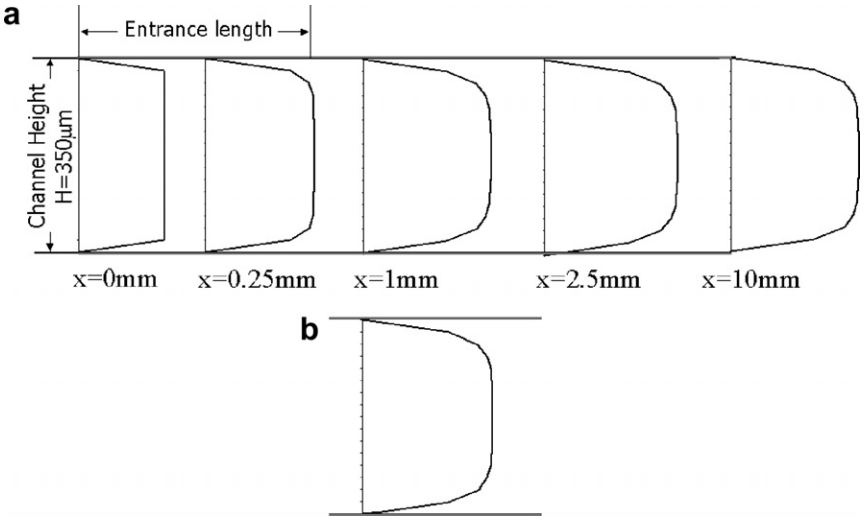


Fig. 3. Velocity profile in the cross-section of the channel at $z = W_{pitch}/2$ along the streamwise ($x$) direction: (a) developing flow; (b) developed flow.

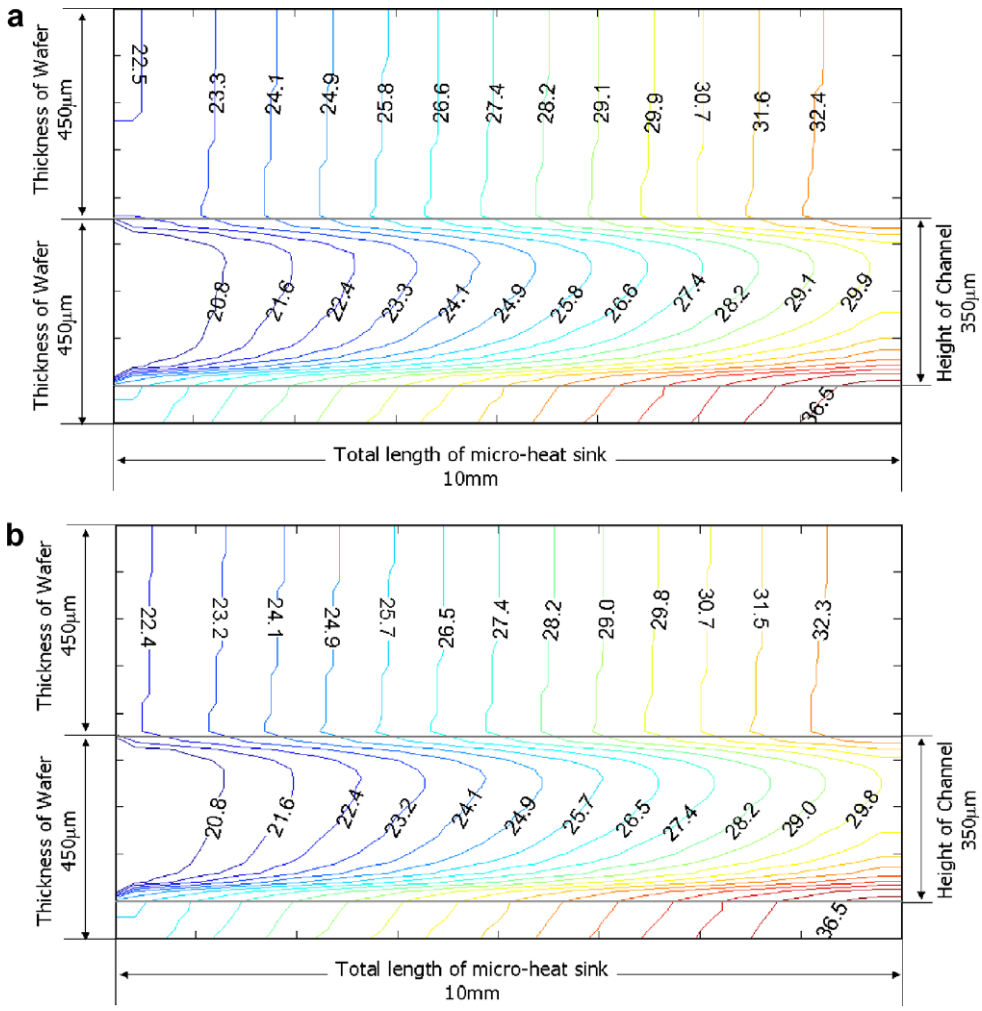


Fig. 4. Comparison of temperature distribution in the cross-section of the microheat sink at $z = W_{\text{pitch}}/2$ between the full 3D numerical simulation and the simplified 3D numerical simulation ($q_w = 100$ W/cm$^2$, $\overline{P} = 0.05$ W): (a) simplified 3D numerical result; (b) full 3D numerical result.

Defining the Fanning friction factor as

$$f = \frac{D_h}{2\rho_l u_m^2}\frac{\Delta P}{L_x} \tag{14}$$

The partial derivative of the non-dimensional momentum governing equation becomes

$$\frac{\partial^2 U}{\partial y^2} + \frac{\partial^2 U}{\partial z^2} = -\frac{2}{D_h^2} Re_{D_h} \cdot f \tag{15}$$

where the hydraulic diameter is $D_h = \frac{2HW}{(H+W)}$. It is important to note that for fully developed, laminar flow, $Re_{D_h} \cdot f$ is constant for a specific channel geometry and thus the non-dimensional velocity is only a function of the geometry of the channel. As indicated in [4,14,15] for fully developed laminar flow, Knight et al. [4] determined that

$$Re_{D_h} \cdot f = \gamma \tag{16a}$$

$$\gamma = 4.70 + 19.64G \tag{16b}$$

$$G = \frac{H^2 + W^2}{(H+W)^2} = \frac{\alpha^2 + 1}{(\alpha+1)^2} \tag{16c}$$

where $\alpha$ is the aspect ratio of the channel, $\alpha = H/W$. Eqs. (16a)–(16c) agree with the exact values provided in the literature [15] within ±3%. Thus Eq. (15) can be solved for any specific geometry.

With the aid of Eq. (16a) and the definition of the Fanning friction factor, Eq. (14), the mean velocity $u_m$ can be described as

$$u_m = \frac{D_h^2}{2\gamma\mu_l}\frac{\Delta P}{L_x} \tag{17}$$

Substituting Eq. (1) into Eq. (17),

$$u_m = \sqrt{\frac{D_h^2}{2\gamma\mu_l}\frac{1}{L_x}\frac{1}{NWH}\overline{P}} = \sqrt{\frac{2}{\gamma\mu_l}\frac{\alpha}{(\alpha+1)^2}\frac{1}{N\cdot L_x}\overline{P}} \tag{18}$$

$\overline{P}$ has an order of magnitude of 0.001–1 W for the realistic situation (corresponding to $\Delta P = 1$ kPa–$1 \times 10^3$ kPa). In order to guarantee fully developed laminar flow, $\overline{P} = 0.05$ W was chosen in the current investigation.

If the following notation is adopted, $\beta = W/W_{\text{pitch}}$, and with the aid of the notation for $\alpha$, Eq. (13) becomes (here $L_x = L_z$)

$$Re_{D_h} = \frac{2\alpha\beta L_z}{N \cdot \upsilon_l(\alpha+1)^2}\sqrt{\frac{2\alpha}{\gamma\mu_l N L_x}\overline{P}} \tag{19}$$

By introducing the following non-dimensional temperature definition, $\theta(x,y,z) = \frac{\lambda_l}{W_{\text{pitch}} \cdot q_w}[T(x,y,z) - T_{l,\text{in}}]$, from the derivation, the semi-normalized energy equations can be described as

$$U\frac{\partial\theta_l}{\partial x} = \frac{D_h}{Pr \cdot Re_{D_h}}\left(\frac{\partial^2\theta_l}{\partial x^2} + \frac{\partial^2\theta_l}{\partial y^2} + \frac{\partial^2\theta_l}{\partial z^2}\right) \quad \text{for the liquid} \tag{20}$$

$$\frac{\partial^2\theta_w}{\partial x^2} + \frac{\partial^2\theta_w}{\partial y^2} + \frac{\partial^2\theta_w}{\partial z^2} = 0 \quad \text{for a homogeneous substrate} \tag{21}$$

and the boundary condition described in Eq. (7a) becomes

$$x = 0, \quad \text{if } (y,z) \in \text{ channel } \theta_l = 0, \text{ else } -\frac{\partial\theta_w}{\partial x} = 0 \tag{22a}$$

and in Eq. (7c) becomes

$$y = 0, \quad -\frac{\lambda_w}{\lambda_l}W_{\text{pitch}}\frac{\partial\theta_w}{\partial y} = 1 \tag{22b}$$

The other boundary conditions are the same, except that the temperature, $T$, is replaced by the dimensionless temperature, $\theta$, in Eqs. (7b), (7d)–(7g). Thus, all of the governing equations (15) and (20), (21), and all of the boundary conditions are only a function of the dimensionless parameters, $\alpha$, $\beta$, and $N$, and the pumping power, $\overline{P}$. With the boundary conditions of Eq. (22), Eqs. (15) and (20), (21) can be solved numerically. The required solution procedure can be summarized as follows:

(1) First, for a given channel number, $N$, the mean velocity $u_m$ and the $Re$ number can be obtained from Eqs. (18) and (19), and the dimensionless 2D velocity profiles can be obtained from Eq. (15), for different values of $\alpha$ and $\beta$;
(2) Then, the dimensionless energy equations, Eqs. (20) and (21), can be solved for different values of $\alpha$, $\beta$ and $Re$.

## 3. Results and discussion

A series of numerical calculations of the dimensionless temperature distribution in a heat sink are developed in this section. The numerical calculations were carried out for the following hydrodynamic conditions, $\overline{P} = 0.05$ W, and for a fixed total dimension of the heat sink, 10 mm × (2 × $T_{\text{wafer}}$) × 10 mm ($L_x \times L_y \times L_z$).

For design purposes, the global thermal resistance is of the greatest interest and hence, the following classical definition of the thermal resistance was used and was written as

$$R_T = \frac{\max(T_w) - T_{l,\text{in}}}{q_w L_x L_z} \tag{22}$$

Using the definition for the non-dimensional temperature, the thermal resistance can also be expressed as

$$R_\theta = \frac{\max(\theta_w)}{N \cdot L_x \cdot \lambda_l} \tag{23}$$

which is a function of only the maximum dimensionless temperature at the bottom surface of the substrate and the number of the channels (here the length of the heat sink and the thermal properties of the liquid are constant). Minimization of this quantity will lead to an optimal design of the heat sink. It should be noted that Eq. (23) does not necessarily imply that the more channels fabricated, the smaller the thermal resistance, because of the effect of the other parameters.

Fig. 5a–d, present the values of the global thermal resistance for the channel heights, $H$ of 350 μm, 500 μm 700 μm and 900 μm with variations in the number of channels per centimeter and variation of the value of $\beta$. The lowest thermal resistance was found at approximately $N = 120$ and $\beta = W/W_{\text{pitch}} = 0.7$; $N = 100$ and $\beta = W/W_{\text{pitch}} = 0.7$; $N = 100$ and $\beta = W/W_{\text{pitch}} = 0.6$; and $N = 80$ and $\beta = W/W_{\text{pitch}} = 0.6$, respectively, which results in approximately 0.162, 0.144, 0.136, and 0.152, respectively, for $\overline{P} = 0.05$ W.

Fig. 6 presents a comprehensive comparison among the lowest values of the global thermal resistance for different channel heights. The optimal structure was found at approximately $N = 100$ and $\beta = W/W_{\text{pitch}} = 0.6$ and $\alpha = H/W = 12$ for $\overline{P} = 0.05$ W.

The reasons for these differences are primarily due to the following aspects. From a detailed inspection of the thermal resistance, Eq. (23) can be rewritten as

$$R_\theta = \frac{\max(\theta_w - \theta_{l,x=L_x} + \theta_{l,x=L_x})}{N \cdot L_x \cdot \lambda_l} = \frac{\Delta\theta_{x=L_x}}{N \cdot L_x \cdot \lambda_l} + \frac{\theta_{l,x=L_x}}{N \cdot L_x \cdot \lambda_l} \tag{24}$$

The first term on the right hand side of the above equation is related to the substrate conduction thermal resistance and the second term is the convection thermal resistance. Basically, since the thermal conductivity in the silicon is high compared to the value for water, the second term will play a more dominant role in the overall thermal resistance. The convection thermal resistance is related to $\propto 1/(A \cdot h)$ [2], where $A$ is the total peripheral area of the microchannel $A = L_x(2H + 2W)$ and $h$ is the convective heat transfer coefficient ($h$ is a function of the mean velocity if all of the other parameters are the same, e.g. the geometry of the channel and the properties of the fluid). If the effect of the conduction resistance on the overall thermal resistance is considered, the different gradients of these curves as shown in Fig. 5a–d, are completely understandable and quite reasonable. The optimal resistance is primarily a compromise between the heat transfer area of the liquid flow, the heat conduction in the substrate and the flow friction.

In order to validate the numerical results of the present study with the existing experimental results available in the

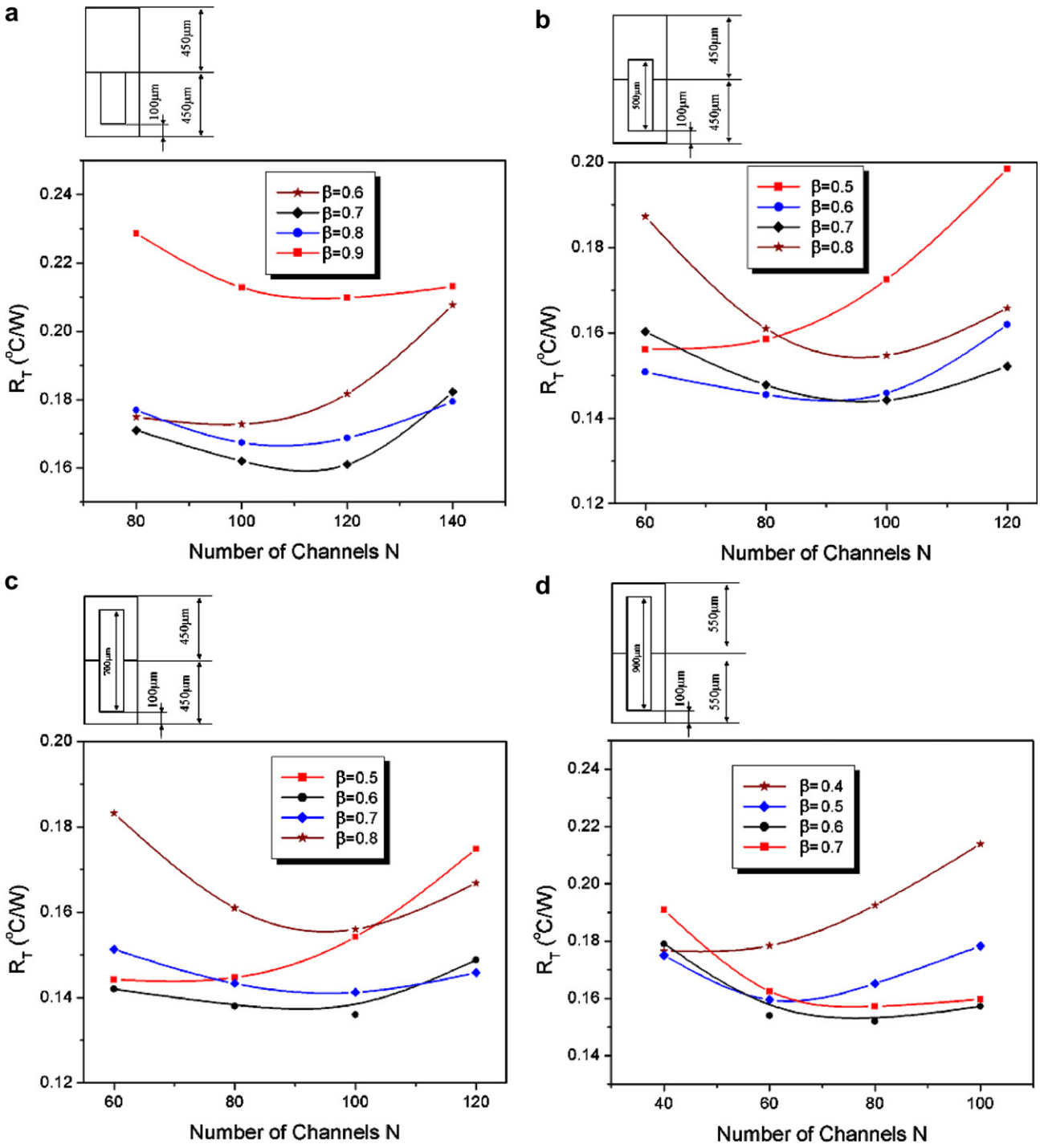


Fig. 5. Comparison of the global thermal resistance for different configurations with variations of number of channels given the height of channel $H = 350$ μm (a), 500 μm (b), 700 μm (c), 900 μm (d).

literature, a series of numerical simulations have been done with the optimized microheat sink to determine the performance of the optimized microheat sink for different pumping powers. Fig. 7 illustrates the temperature distribution in the optimized microheat sink under a heat flux of 1000 W/cm$^2$ and a pumping power of 2 W (which was the highest pumping power used in the investigation of Tuckerman and Pease [2]), and Fig. 8 shows the average temperature of the bulk liquid and the substrate wall along the streamline direction ($x$-direction). The average temperatures can be defined as

$$\overline{T}_{\mathrm{w}}(x) = \frac{\sum_{k=1}^{n} T_{\mathrm{w}}(i, j=1, k)}{n} \quad \text{for the bottom wall} \tag{25}$$

$$\overline{T}_{\mathrm{l}}(x) = \frac{\sum\sum \rho_{\mathrm{l}} u(i,j,k) C_P T_{\mathrm{l}}(i,j,k) \Delta y \Delta z|_{(j,k)\in \mathrm{Channel}}}{\dot{m} C_P}$$

for the bulk liquid (26)

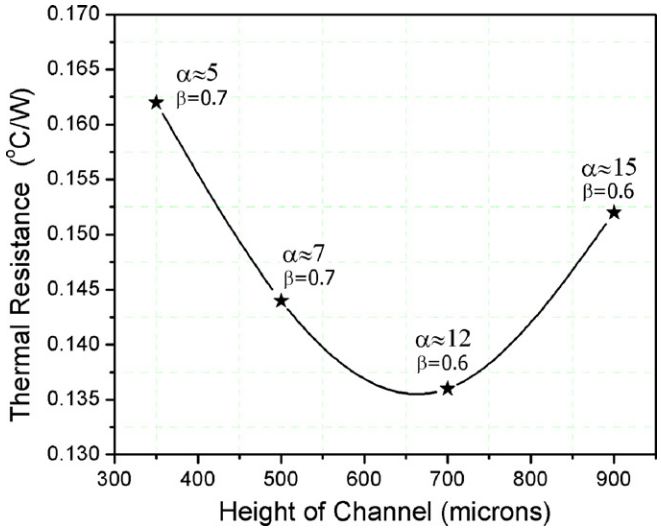


Fig. 6. Comparison of the lowest thermal resistance for the different heights of the channel under the pumping power $\overline{P} = 0.05$ W.

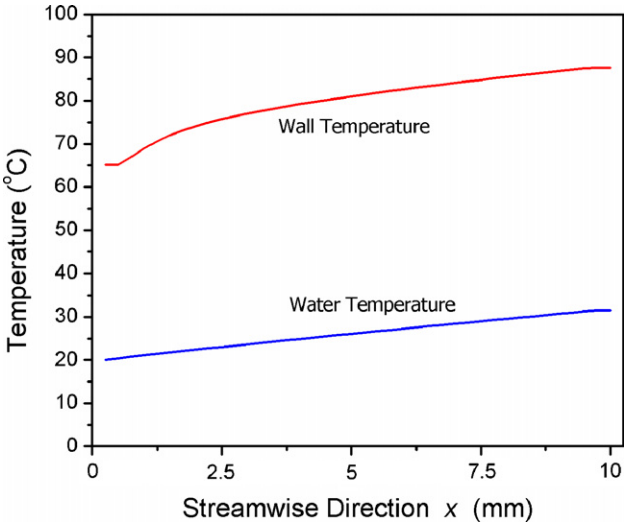


Fig. 8. The variations of the averaged temperature of the bulk liquid and the substrate bottom wall along the streamwise direction for the case as shown in Fig. 7.

The difference between the highest temperature on the bottom wall and the lowest value of the bulk liquid is nearly equal to the junction temperature difference. Here, the inlet temperature of the liquid was assumed to be 20 °C and the difference in the bottom wall temperature along the $z$-direction was not significant, due to the high thermal conductivity of silicon. The value obtained if this temperature difference is divided by the heat flux yields the global thermal resistance (or junction thermal resistance). From Fig. 8, a low thermal resistance of 0.068 is obtained.

Fig. 9 illustrates the comparison between the numerical results for the optimized microheat sink and the experimental results of Tuckerman and Pease [2] with the respective geometric configurations under different pumping powers. In Fig. 9, Curve 1 shows the numerical results for the optimal microheat sink ($H = 700$ μm, $W = 60$ μm, $W_{\text{pitch}} = 100$ μm, and $\delta = 100$ μm fabricated on two 450 μm silicon wafers bonded together by direct bonding method with double side alignment), and Curve 2 shows the numerical results for the configuration utilized by Tuckerman and Pease, i.e., $H = 300$ μm, $W = 50$ μm, $W_{\text{pitch}} = 100$ μm,

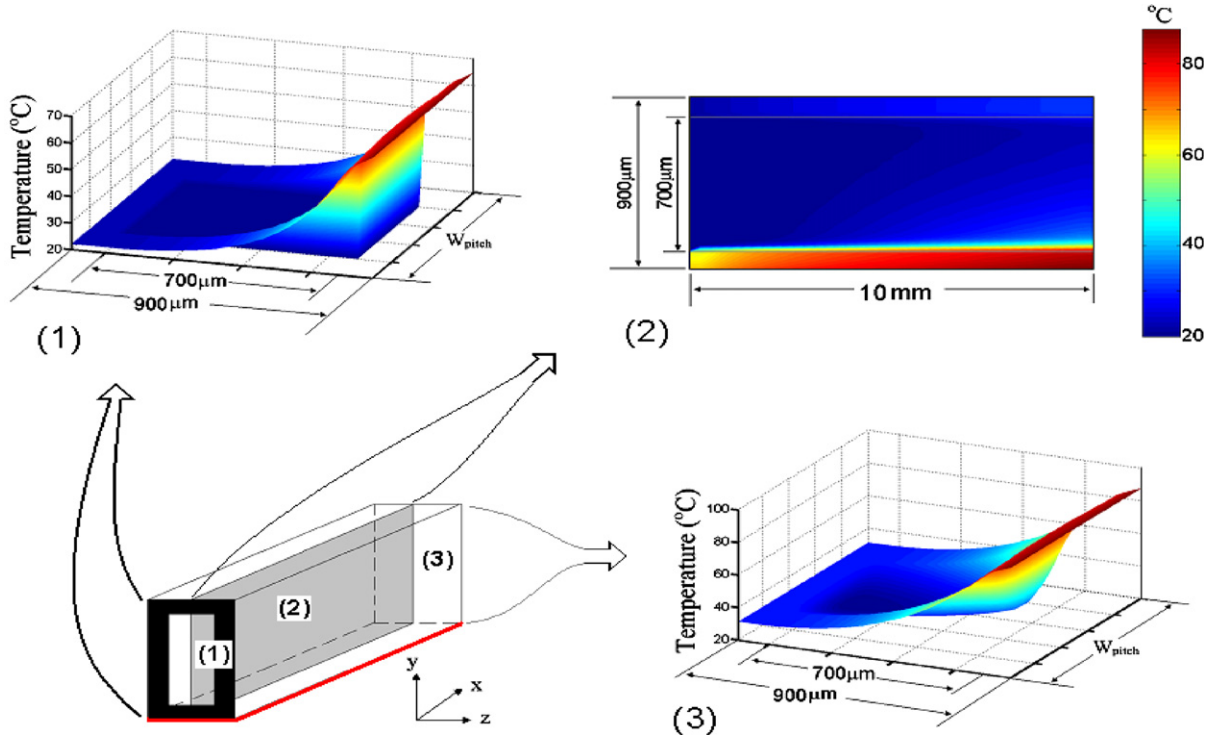


Fig. 7. Temperature distribution in the optimized microheat sink for $q_w = 1000$ W/cm$^2$ and $\overline{P} = 2.0$ W.

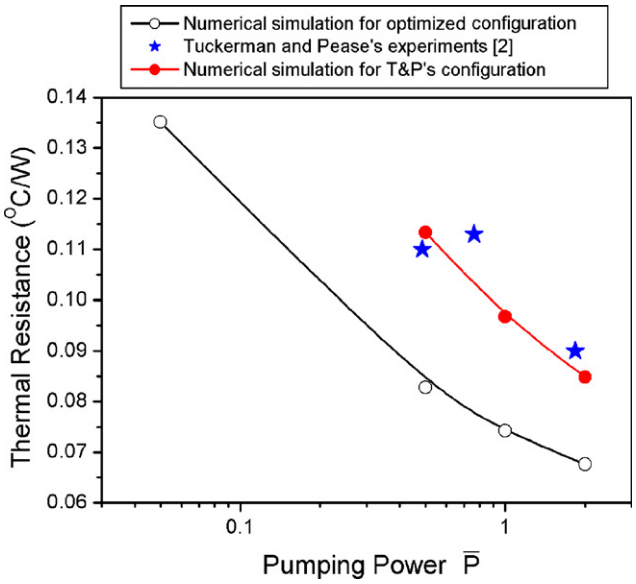


Fig. 9. The relationship between the thermal resistance and the pumping power for the optimized heat sink and the comparison between the numerical calculations and the experimental results of Tuckerman and Pease [2].

$\delta = 100$ μm, fabricated on a 400 μm silicon wafer anodically bonded with a Pyrex glass cover, with the full 3D numerical method, where the stars represent the Tuckerman and Pease experimental results. If the numerical solution error discussed previously of 6% is used and the experimental uncertainties are considered, the present numerical approach shows good agreement with the experimental data. From the comparisons among the calculations and experiments, it is obvious that the heat transfer performance with the optimal geometry obtained in this study is improved noticeably above the Tuckerman and Peace's configurations with an averaged improvement more than 20%.

## 4. Concluding remarks

In the preceding analysis, a full 3D numerical simulation for fluid flow and heat transfer in parallel microchannel heat sink was developed and used to evaluate and determine the optimal geometric conditions. The results indicate that for relatively low pumping powers, the fully developed flow assumption will introduce a very small and negligible error in the global thermal resistance calculation. The numerical model was validated by comparison with existing experimental data available in the literature and the resulting partially dimensionless, simplified 3D numerical approach for a low pumping power situation was used to determine the dimensionless temperature and the global thermal resistance of the microheat sink. By optimizing the geometry, based upon the minimized thermal resistance, the preferred geometry of the microheat sink for a pumping power of 0.05 W was determined to be $N = 100$/cm (or $W_{\text{pitch}} \approx 100$ μm) and a ratio of $\beta = W/W_{\text{pitch}} = 0.6$ (or $W \approx 60$ μm) with an aspect ratio of $\alpha = H/W \approx 12$ (or $H \approx 700$ μm).

The 3D analysis performed here provides a full understanding of the effects of the geometry of the channel on the heat transfer capacity of these types of heat sinks. Through a detailed comparison with the published benchmark experimental data, improvements in the heat transfer performance using an optimal geometry were found to be significant and not limited by current fabrications restrictions as previously hypothesized. The results are applicable in a wide variety of applications with specific application to the microelectronics industry.

## Acknowledgements

The authors would like to acknowledge the support of the Office of Naval Research Grant ONR N0001400104-54 and the National Science Foundation CTS-0312848. The authors would like to acknowledge the work of Ms. Ummikalsom Abidin at the University of Technology – Malaysia for her review of the model developed herein.

## References

[1] S.P. Gurrum, S.K. Suman, Y.K. Joshi, A.G. Fedorov, Thermal issues in next-generation integrated circuits, IEEE Trans. Dev. Mater. Reliab. 4 (4) (2004) 709–714.
[2] D.B. Tuckerman, R.F.W. Pease, High-performance heat sinking for VLSI, IEEE Electron. Dev. Lett. EDL-2 (1981) 126–129.
[3] R.W. Knight, J.S. Goodling, D.J. Hall, Optimal thermal design of forced convection heat sinks—analytical, ASME J. Electron. Packag. 113 (3) (1991) 313–321.
[4] R.W. Knight, D.J. Hall, J.S. Goodling, R.C. Jaeger, Heat sink optimization with application to microchannels, IEEE Trans. Compon. Hybrids Manufact. Technol. 15 (5) (1992) 832–842.
[5] H.H. Bau, Optimization of conduits' shape in micro heat exchangers, Int. J. Heat Mass Transfer 41 (1998) 2717–2723.
[6] C. Perret, J. Boussey, C. Schaeffer, M. Coyaud, Analytical modeling, optimization, and realization of cooling devices in silicon technology, IEEE Trans. Compon. Packag. Technol. 23 (4) (2000) 665–672.
[7] L.T. Hwang, I. Turlik, A. Reisman, A thermal module design for advancing packaging, J. Electron. Mater. 16 (5) (1987) 347–355.
[8] A. Weisberg, H.H. Bau, J.N. Zemel, Analysis of microchannels for integrated cooling, Int. J. Heat Mass Transfer 35 (1992) 2465–2474.
[9] J.H. Ryu, D.H. Choi, S.J. Kim, Numerical optimization of the thermal performance of a microchannel heat sink, Int. J. Heat Mass Transfer 45 (2002) 2823–2827.
[10] J. Li, G.P. Peterson, Geometric optimization of a micro heat sink with liquid flow, IEEE Trans. Compon. Packag. Technol. 29 (1) (2006) 145–154.
[11] K. Kawano, K. Minakami, H. Iwasaki, M. Ishizuka, Development of micro channels heat exchanging, in: R.A. Nelson Jr., L.W. Swanson, M.V.A. Bianchi, C. Camci (Eds.), Application of Heat Transfer in Equipment, Systems, and Education, HTD-Vol. 361-3/PID-Vol. 3, ASME, New York, 1998, pp. 173–180.
[12] S.V. Patankar, Numerical Heat Transfer and Fluid Flow, Hemisphere, Washington, DC, 1980.
[13] J. Li, G.P. Peterson, P. Cheng, Three-dimensional analysis of heat transfer in a micro heat sink with single phase flow, Int. J. Heat Mass Transfer 47 (2004) 4215–4231.
[14] A. Bejan, Convective Heat Transfer, first ed., John Wiley & Sons, New York, 1984.
[15] W.M. Kays, M.E. Crawford, Convective Heat and Mass Transfer, McGraw-Hill, New York, 1990.